December 23, 2018

ÉCOLE POLYTECHNIQUE
FÉDÉRALE DE LAUSANNE

FLEXIBLE BIOELECTRONICS PROF. STÉPHANIE LACOUR, PHD

A Novel Approach To Aortic Restenosis

Furrer Stanislas, Carla Nannini, Brooke Zampell, Francesco Morandini

Table of Contents

Abstract

Aortic stenosis, a narrowing of the valve where blood exits the left ventricle, is one of the most common cardiovascular diseases in the Western world. It occurs in 2-7% of people over 65 years old, and its prevalence is increasing as the human lifespan continues to lengthen [1]. This disease degrades quality of life and greatly increases chances of sudden death. Treatment options include aortic valve replacement and balloon valvuloplasty, depending on the severity of the condition and the age of the patient [2]. Restenosis is unfortunately a common complication after treatment; among those who receive a balloon angioplasty, restenosis has approximately a 23% rate among the population, and often occurs less than 12 months after treatment [3]. To date, no device is on the market which performs early detection of restenosis. One of the ways this condition can be detected is through the drop in systolic pressure within the ascending aorta, which is the section of aorta immediately after the aortic valve (Figure 1). With early detection, the condition can be properly treated before it reaches life-threatening levels.

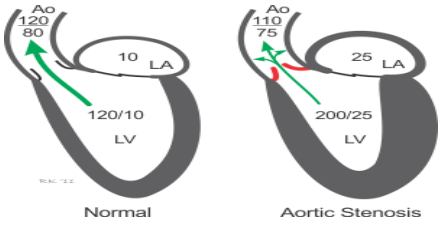

Figure 1: Pressures [mmHg] in the left side of the heart in a healthy patient (left) and a patient with aortic stenosis (right). Notice the rise in aortic pressure in the case of aortic stenosis. Image source: Cardiovascular Physiology Concepts

The goal of our device is to address the need for early and precise detection of aortic restenosis immediately following stenosis treatment surgery. The device consists of two parts: an implanted pressure sensor and an external chest patch. The wireless internal pressure sensor is attached to an endovascular aortic stent and communicates with the chest patch via radio frequency (RF). The entire internal component does not require a power source. The pressure sensor that we wish to develop is a capacitive pressure sensor with an LC circuit that corresponds to an RF tag. The implantable circuit will have dimensions of 4x4 mm^2 and a thickness of about 60 microns.

With the biodegradable need in mind, we chose to make the capacitor of our pressure sensor out of magnesium (Mg) plates and a dielectric of polyglycerol sebacate (PGS). The RF coil will also be made of Mg. Mg was a simple choice; zinc and Mg are the most commonly used biodegradable metals, and Mg has a higher conductivity than zinc. The substrate is polylactic acid (PLA), with a barrier encapsulation of poly(octamethylene maleate (anhydride) citrate) (POMaC). POMaC enables the tuning of the device's lifetime, which will be approximately 6 months before loss of function. This biodegradability ensures that restenosis within the riskiest period immediately after surgery will be detected, but the device is not in the body longer than necessary.

A patch on the thorax will sound both LC circuits. This will allow us to measure the variation of the impedance of the exciter circuit; using the Todd-Andrews algorithm, we will be able to find the peaks within the noisy data, producing values for pressure inside the aorta. Finally, the graphs of systolic and diastolic pressures of aortic and ventricular pressure can be plotted. We can thus compare these two pressures in order to deduce if there is a stenosis and if so, how severe it is. The pressure sensor will be micro-machined using standard microfabrication processes.

State of the Art Review

In recent years, intelligent implantable sensors have been identified as a key research area for microtechnology and electronics. These sensors enable accurate physiological monitoring without limiting the mobility of the patient (or research animal). Some of these implantable sensors take advantage of RF technology, a passive communication and data transmission method which does not require a battery. An RF tag is composed of two circuits that work together, each possessing a coil. A transmitter sends, via a generator coil, a magnetic field oscillating on its LC circuit. At a given frequency, this LC circuit resonates, modifying in return the impedance of the generator coil and thus transferring data from the variable capacitor between the two circuits (Figure 2). The resonance frequency is calculated using the following formula:

$$\omega_0 = 2\pi f_0 = \frac{1}{\sqrt{L_s C_s}}$$

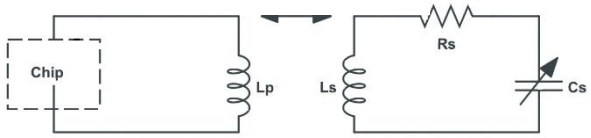

Figure 2: Inductive-capacitive resonant circuitry for RF technology. On the right, a circuit with a variable capacitor measures the blood pressure via changes in capacitance. This data is then transmitted wirelessly and without a battery to the circuit on the left, which is integrated into an external chest patch, via RF communication. The patch then performs data analysis.

Since changes in either capacitance or inductance can modify the resonant frequency, the key to accessing changes in the capacitance, and thus to measuring a pressure difference, is to choose a frequency at which the inductance of the coil remains constant after fabrication. Figure 3 demonstrates the changes in inductance as a function of frequency. We can see that by applying a frequency greater than 14 MHz, the inductance of the generator coil is modified allowing us to work in the range of frequencies between 14.45 MHz and 15MHz.

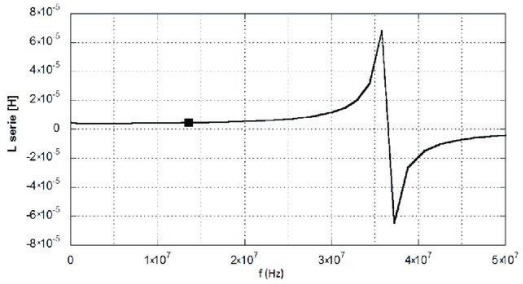

Figure 3: Changes in inductance relative to radio frequency. The marker (black square) indicates the frequency beyond which the inductance of the generator coil is no longer constant. In this example, the inductance starts to change at 14MHz.

The literature is populated with several devices which measure blood pressure and communicate these readings with an external reader, applying the theory of RF or similar technology. There are two devices of note. Caldara et al. [4] proposed a blood pressure sensor which utilizes radio frequency identification (RFID) technology to take short-term measurements in animal experimentation. The ultimate goal is to develop this device to the point where it can be used in research studies that last approximately 10 days, measuring the average, systolic and diastolic blood pressure of a laboratory animal, once every minute for the length of the study. This miniaturized, compact device is composed of a pressure sensor membrane, a microcontroller, non-volatile memory storage, RFID technology, and

a Lithium ion battery. Data is processed by the on-board microcontroller, utilizing the Todd-Andrews algorithm to identify peaks. The required battery as well as the RFID tag, which receives the signal from the miniaturized device, would be located under the animal's cage. The final device was integrated with a catheter for use in vivo. Initial testing of the device was performed using a sphygmomanometer to exert air pressure. The device was then characterized in vivo by inserting the catheter into the femoral artery of rats and taking 20 seconds of data.

Caldara's device could be an innovative solution for monitoring animal research while allowing the animals to retain free movement. Since the device has not yet been developed to the point of being inserted into the animal, all electronics components being used for RFID are made of standard electronics materials that are neither flexible nor biodegradable. The two-layered printed circuit board enables the miniaturization of the device.

The other notable pressure sensor in the literature, presented by Chen et al. [5], serves as a monitor for in-stent restenosis, an event that frequently occurs after the insertion of a stent in which the blood vessel's endothelial cells grow over the stent, further occluding the vessel and requiring a second treatment. Chen designed a micro-electromechanical systems (MEMS) sensor which functions as a capacitive pressure sensor, coupled with a metal stent. This paper focused on clinical usability for coronary artery stenting. The sensor is composed of a stainless-steel substrate which also serves as one of the electrodes, a flexible diaphragm made of gold-titanium-polyimide which comprises the other electrode, and a reference capacity between these two electrodes. All stainless-steel components were micromachined. The multilayered flexible electrode was manufactured by electron-beam evaporation of titanium and gold onto a temporary copper substrate, then spin coating of polyimide onto the titanium. Thermal bonding of the two electrodes was followed by etching to remove excess layers.

The completed sensor was then microwelded onto a stainless-steel stent. The stent, which was electroplated with gold to reduce the series resistance of it and then covered in Parylene C for biocompatibility, functions as an electrical inductor or antenna for radiofrequency (RF) communication. A handheld external wireless reader is then used to interrogate the implanted sensor. Since Chen's device uses passive RF technology, no battery is necessary. The prototype was successfully tested in a swine model, where artificial alterations in blood pressure produced the expected shifts in resonant frequency of the sensor. During testing, a blood clot unintentionally formed within the stent and the pressure readings increased, indicating that the stent indeed can detect biological phenomena.

One other device which is relevant to our proposed product is the Gore Ascending Stent Graft. This fabric-covered stent is a treatment for the condition of aortic dissection and is placed in the ascending aorta [6]. There is no pressure sensor on this stent, but such a clinically marketed device is important to mention because it proves the feasibility of placing a stent within the ascending aorta, an idea which we initially thought to be too risky due to its proximity to the heart.

Our Novel Approach

Although the previous devices by Caldara and Chen are intriguing, they leave much to be desired. Caldara's sensor utilizes RFID technology, which means the sensor must contain a chip; chips cannot currently be made out of biodegradable materials and thus are a permanent addition to the body. As discussed previously, the body is prone to negative immune or clotting reactions against artificial materials that are left in the body long-term. The specific RFID device used here also necessitates the presence of a battery, which is an inconvenience. Additionally, this device is only made for a few days of use maximum, and no biocompatible coating has yet been specified for the sensor. Regarding Chen's paper, the proposed sensor is also non-biodegradable as it contains stainless steel. The partially steel sensor is non-flexible, making for limited applications and delivery systems. The stent, which serves as an RF coil, must also thus be made of metal and is not degradable. With these flaws in mind, neither of these devices can be applied to early aortic restenosis detection. A market opening clearly exists for

such a device which can alert a patient to restenosis before adverse symptoms set in and which does not require a permanent placement in the body. Our device can fill this market gap.

Capacitive Pressure Sensor Design

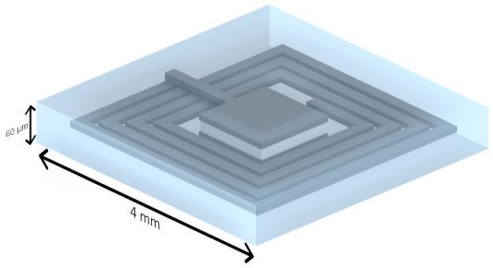

Figure 4 : Capacitive Pressur Sensor

The device design begins with a capacitive pressure sensor which reads blood pressure in the ascending aorta. The capacitor must be made of biodegradable materials which have desirable electrical properties and are also mechanically soft such that the capacitor can deform and change its capacitance. These requirements led us to choose magnesium (Mg) for our plates and polyglycerol sebacate (PGS) as the dielectric.

Magnesium is a straightforward choice. The main metals which are biodegradable include magnesium, zinc, tungsten, iron, molybdenum, and their oxides. Zinc and Mg are most commonly used due to their easy processing properties and the higher concentration tolerance that the body has for them [7]. Between these two, Mg was chosen because it has better conductivity: Mg's value $2.15 \cdot 10^7$ S/m and zinc's is $1.69 \cdot 10^7$ S/m

The dielectric was a much trickier choice. Based on Matlab calculations which will be detailed later, we needed to keep it thin to minimize stress on the capacitor plates, while also requiring a very compressible material (compressive modulus of less than 1 GPa) in order to have good sensitivity to pressure changes. Many polymers which satisfy the requirements of a dielectric are too stiff. PGS, however, is a bioresorbable thermoset polyester which exhibits elastomeric properties, has a tunable compressive modulus of 0.05-2 MPa, and has been investigated for use as a biodegradable dielectric [8].

The one unfortunate aspect of this choice is that the dielectric constant is currently unknown due to lack of testing in the literature. We attempted contacting authors of papers that have used PGS in an electrical context, but none of them replied. Since no other polymers possess the Young's modulus that was required and we knew that PGS has been used as a dielectric successfully, we decided to incorporate PGS into our device and use a proxy value from another polymer as its dielectric. This approximation was guided by the advice of Dr. Rodney Stramel, a bioprinting chemist PhD. The dielectric constant range for glycerol phthalate as well as esters of triocetate at 20°C is approximately 3-6, depending on processing method of the material. Dielectric constants decrease as temperature increases, and the body temperature is 37°C. We can thus hypothesize that the dielectric constant of glycerol sebacate is slightly lower than this range, and its condensation polymer, PGS, has a similar value [9]. We therefore took this value to be 2.65 F/m. The dimensions of the capacitor are determined later in the design process since they depend on other variables.

Since Mg has an extremely quick degradation rate, an encapsulation layer which serves as a hermetic seal and thus maintains the device's functionality for a longer period of time is necessary. The encapsulation must be thick enough to extend the device's lifetime, but also thin and soft enough such that it can deform and therefore not significantly reduce the capacitor's sensitivity. This layer's softness is also important because the more extreme curvature that the sensor must withstand when the stent is collapsed before deployment means the encapsulation layer must be flexible. We chose to meet these requirements using a combination of materials; PLA (Young's modulus of 1 GPa[34]) meets the mechanical needs, while a barrier encapsulation of POMaC provides the hermetic seal.

RF Communication System

With the capacitive pressure sensor and its hermetic sealant designed, we move on to the RF communication system, whose Mg coil will also be within the encapsulation layer. One of the first

choices to make for this miniaturized implantable RF tag system is the resonant frequency, due to the existence of several restrictions associated with the use of RF technology. The two main limitations are signal dissipation and in vivo effects on the human body.

Signal dissipation is important for our device because the internal pressure sensor must communicate through the body with the external chest patch. Considering that the anterior aortic wall is an average of 1.9 cm from the sternum and the aorta has a diameter of 2.0 cm, the signal must be sent through 2.9 cm of human tissue [10].

Various studies have shown that in the range of 1-20 MHz, electromagnetic waves are not significantly attenuated through tissues, and thus our frequency will be within this range [11]. To find an exact frequency, we examine the attenuation properties of an electromagnetic wave in a dielectric, which are described by a property known as "skin depth" δ.

$$\delta = \sqrt{\frac{2}{\omega\mu\sigma}} \qquad \begin{array}{ll} \sigma : Conductivity\ [S/m] & \delta : Skin\ depth\ [m] \\ \omega : Angular\ frenquency\ [rad/s] & \mu : Magnetic\ permeability\ [H/m] \end{array}$$

The general idea of our project is to be able to measure systolic and diastolic pressure in humans. It is possible in particular to transmit with such frequency, information over a distance of about 10 cm, through the human body [12][13].

To meet the in-vivo effects limitation, the biological response of an RF magnetic wave is found by calculating the specific absorption rate (SAR). This is a measure of the rate at which energy is absorbed by the human body (mass tissue) when exposed to a radiofrequency (RF) electromagnetic field, in watts per kilogram W·kg^{-1}. It is given by the following formula :

$$SAR = \frac{\sigma \cdot E^2}{\rho} \qquad \begin{array}{l} \sigma : Electrical\ conductivity\ of\ the\ tissues\ [S \cdot m^{-1}] \\ E : Electrical\ field\ [V \cdot m^{-1}] \\ \rho : Density\ of\ the\ tissue\ [kg \cdot m^{-3}] \end{array}$$

The International Commission on Non-ionizing Radiation Protection (ICNIRP) sets a SAR safety limit for the whole body of 2 W·kg^{-1}, above which they consider that there is damage to the body. We were able to determine the various body tissues' dielectric properties. For the frequency of 15 MHz that is used for our device, the following values for the heart tissue were found [5] :

$$\sigma = 0.659199\ S \cdot m^{-1} \text{ and } \rho = 1040\ kg \cdot m^{-3}$$

Using the ICNIRP guidelines [6], we found that for a frequency range of 10-400 MHz, the electric field is 28 V·kg^{-1} . This value leads to the calculation of the SAR for heart tissue as 0.403 W·kg^{-1}, which can be translated to an average signal transmission time of 6 minutes per hour. This is well below the safety limit. Thus, it will be considered that for a frequency of the order of 15 MHz, there is no negative impact on the human body. Our device will therefore be taking measurements for 6 seconds every minute, in order to meet these requirements

Inductance Calculation

As previously mentioned, the inductance of the coil remains constant after fabrication. It is therefore possible to calculate it. We limited our LC circuit including the pressure sensor, to a surface of 4x4 mm2 for a thickness of 60 microns. We will set the loop number of the planar coil to 20 and assume a width and loop thickness of 1 µm. Knowing that our planar coil is rectangular, one can calculate the theoretical inductance Ls thanks to the following formula [7]:

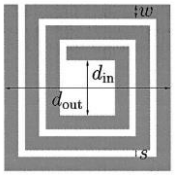

Figure 5 : square inductor coil calculation factors

$$L_s = \frac{1.27 * \mu n^2 d_{avg}}{2}\left[ln\left(\frac{2.07}{\rho_s}\right) + 0.18\rho_s + 0.13\rho_s^2\right] = 3137[nH]$$

$$\begin{array}{l} d_{out} = 3.8\ [mm] \\ d_{in} = 3\ [\text{mm}] \\ n = 20\ tours \\ \mu = 4\pi * 10^{-7}[\text{T m/A}] \end{array} \qquad \begin{array}{l} p_s = (d_{out} - d_{in})/(d_{out} + d_{in}) \\ d_{avg} = 0.5(d_{out} + d_{in}) \end{array}$$

Knowing the inductance at rest as well as the resonance frequency, it is therefore possible to determine the capacity as well as the thickness of the dielectric according to the following formulas:

$$C_0 = \frac{1}{L_s(2\pi f_0)^2} = 35.8\ [pF]$$

$$t_0 = \frac{\epsilon_r \epsilon_0 A}{E_{PDS}} = 4.08\ [\mu m]$$

$$With \quad \begin{vmatrix} \epsilon_0 & = 8{,}8541\ [Fm^{-1}] \\ \epsilon_r & = 2.65 \\ A & = 2.5 \cdot 2.5\ [mm^2] \\ E_{PGS} & = 0.282\ [MPa] \\ f_0 & = 15[MHz] \end{vmatrix}$$

Remark :

The choice of the thickness of the coil comes from a geometric constraint. Note in Figure 4 that the coil is fixed on the plates of the capacitance. Therefore, the thickness of the coil must be at least 3 times smaller than the thickness of the dielectric contained in the capacitor in order not to require bridging using an additional metal contact layer. Thus, we selected a thickness of 1 µm, as a commonly used value range [7]. Impedance, capacitance and dielectric thickness given are the resting values of our system. No aortic pressure is applied yet.

Patch Calculation

The external patch will contain a planar coil. The distance between the external patch and the aortic sensor is x = 29 mm, the internal radius is $d_{in,patch}$ = 5 mm and the external radius is $d_{out,patch}$ = 7 mm. Furthermore, the number of spires is n = 15. Therefore, we can calculate the inductance of our external coil with the previous formula as: $L_p = 2750.1\ [nH]$.

The coupling factor is: $k(x) = \frac{Re^2 \cdot Rtag^2}{\sqrt{Re \cdot Rtag} \cdot \left(\sqrt{x^2 + Re^2}\right)^3} = 0.078$ with $R_{tag} = 3.8$ [mm].

Finally, we can find the mutual inductance of the two coils: $L_m = k\sqrt{L_p \cdot L_s} = 23.03\ [nH]$

Passive sensors are powered through the mutual inductance between the external coil and the sensor coil. The integrated inductor coil supplies the electric power required inside the sensor using the electromagnetic field generated by the external antenna. A bigger inductor coil collects more power for the sensor and vice versa.

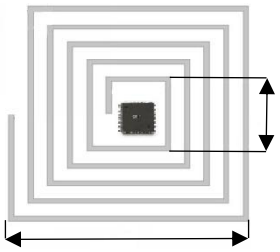

Figure 6 : Patch design. The microcontroller sits at the center, with a surrounding planar coil.

Range of variation

At this point, we know all the initial values of our system. We will apply to it, a pressure range of 0 to 150 mmHg. This is the operating range of the blood pressure sensor at normal blood pressure condition. Thanks to the formula below, it is possible to calculate the dielectric thickness difference as a function of the applied pressure.

$$\Delta t = \frac{t_0 \sigma}{E_{PDS}}$$

This equation allows us to obtain the order of magnitude of variation of the various parameters of our system as well as the range of useful excitation frequencies of it. The three graphs in Figure 7 are derived from this approach.

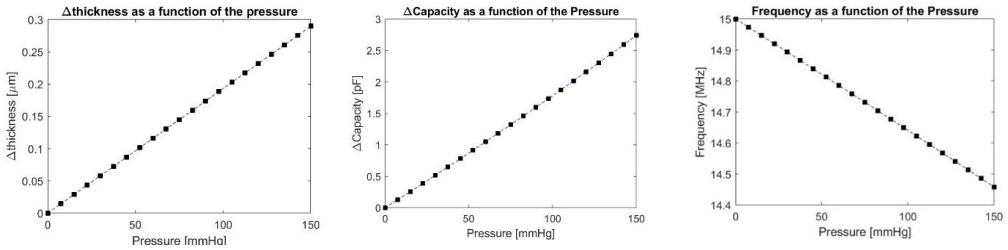

a) b) c)

Figure 7 : Variation de capacité et d'épaisseur en fonction de la pression. Fréquence d'excitation en fonction de la pression. The pressur range tested correspond to a normal blood pressure condition

As the thickness change is relatively small, the various graphs of Figure 7 can be considered as linear over the useful pressure range. According to Figure 7 graph c, the utility range of frequency is between 14.45 and 15 MHz.

Microcontroller

At this stage, the theoretical model of our device is known. It is therefore possible to process our signal. This processing will be done through a 16-bit Arm7 microcontroller MSP432P4111IPZ [x]. This microcontroller has a low price, but also the specificities sought. Indeed, it contains a digital analog converter, can generate frequencies up to 48 MHz and contains an internal memory of 2 MB.

The firmware has been implemented in such a way that the microcontroller acquires pressure sensor data for 6 s. First, it converts the analog signal into digital. This digital signal is then filtered through a bandpass. It is necessary to filter the high frequencies to remove noise and also the low frequencies to remove effects from the patient's breathing. The microcontroller then applies the Todd-Andrews algorithm, a solution to the common problem of peak identification in noisy physiological signals, for the maximum and minimum detection and computes the average systolic and diastolic pressure values. Finally, the microcontroller stores the results on the non-volatile memory. After this phase, the microcontroller enters a stand-by mode for 54 seconds and successively wakes up thanks to the internal real-time clock (RTC).

Test

When writing a scientific paper [xxx], engineers measured the aortic pressure of 3'325 healthy subjects to make a database for research. One of their 6-second samplings was used to test our theoretical model, illustrate the noise problem, and use the peak search algorithm.

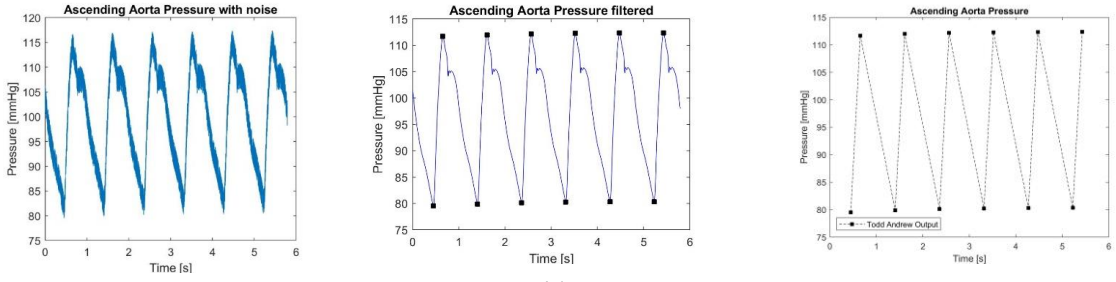

a) b) c)

Figure 8 : Ascending aortic pressure at the input of the microcontroller then treated (a) ascending aorta pressure with noise, (b) ascending aorta pressure filtered with a passband, (c) Peaks of systolic and diastolic pressure

Unfortunately, the study providing the database has already filtered their patient's breathing. For this reason, on figure 8, we do not see the modulation caused by breathing.

Clinical Use and Deployment

To prepare the pressure sensor for clinical use, it must be mounted on a bioresorbable stent. This stent must outlast the sensor to ensure that the stent does not degrade first and thus leave the remains of the sensor free to float down the aorta, likely leading to a clot formation. Among the choices available for stents, the best is a poly-l-lactic acid (PLLA). Clinical trials are currently being run on the most successful PLLA and drug-eluting stent, the Abbott Absorb; empirical testing shows a lifetime of 2-3 years[23]. The DESolve stent from Elixir Medical is another PLLA stent, with a lifetime of 1-2 years [23]. Since these stents are commercially available, we can easily purchase them for use with our device.

The final step in manufacturing is to attach our pressure sensor to the inside of the collapsed stent. A potential biodegradable adhesive with which to perform this task is an isocyanate end-capped polyether copolymer of polyethylene glycol (PEG) and polypropylene glycol (PPG). By fluorinating the aliphatic isocyanate, the adhesive lasts much longer (up to 20 months), which is desirable in our case in order to ensure that the adhesive does not degrade before the sensor [21, 22]. Deployment into the patient would be a simple process which follows any stenting procedure (Figure 9).

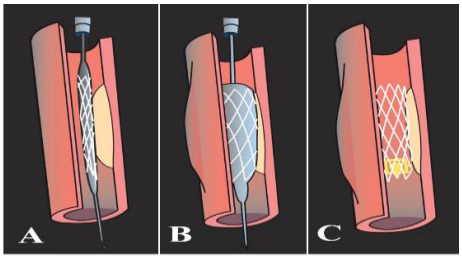

Figure 9: Standard stenting procedure as applied to our device. (A): The collapsed stent is first placed onto a catheter. This catheter is inserted into the femoral artery via a small incision in the thigh, and snaked up the blood vessel network to the desired stent location. (B): The balloon is inflated, permanently opening the stent and pushing it against the artery walls. (C) The balloon is then deflated and removed, leaving the stent in place.

Degradation of Materials

We chose to use biodegradable materials for several reasons. Firstly, as previously stated, restenosis is only a major risk during the first 12 months after the operation. The added bonus of a bioresorbable stent as opposed to the standard, permanent metal stent is that it eliminates long-term risks of blood clots and changes in shear stress experienced by the vessel's endothelial cells, which can lead to abnormal wound-healing response and inappropriate remodeling of the blood vessel once the stent has been in place longer than a year [18]. An important note about biodegradability is that the rate can vary for a single material, depending on many factors such as how the material is processed and whether it is combined with any other materials. As such, while we have found literature values which give the desirable degradation rates, we would need to manufacture and then empirically test our device to be sure that the degradation occurs within the desired time frame. This could be a future improvement should more work be done to develop this device.

The most important factor to control for the biodegradation is the degradation rate of each material relative to the others. The sensor must degrade first, followed by the stent which holds the sensor in place. The encapsulation layer on the sensor controls how long the device remains functional.

Mg dissolves at a rate of 19-44 mg per cm^2 per day within simulated body fluid. This means surface areas can be a maximum of 9-21 cm^2 in order to not exceed the daily exposure limit for an adult of 350-400 mg [19]. Sheets of PGS, the dielectric material, degrade at a rate of 0.2-1.5 mm·$month^{-1}$ [19]. Since our dielectric will be 4.08 μm thick, if we assume the degradation rate to be the average of the range at 0.85 mm·$month^{-1}$, the dielectric layer will degrade entirely upon exposure within days.

PLA has a half-life of roughly 7 months [26]. It loses roughly 17% of its mass in 16 weeks in vivo [27]. Since PLA can only maintain a good barrier for a limited amount of time, the active lifetime of our device is essentially controlled by the POMaC encapsulation, after which the device quickly stops working, due to the Magnesium dissolving.

Degradation of POMaC, which we chose as our barrier material, can be tuned (12 weeks - several months)[estimate from degradation in PBS, 30, 31] by varying the UV exposure of pre-POMaC, in our case, considering the timescale of restenosis, we decided to opt for 6 months degradation time.
Once the POMaC has degraded, PLA will rapidly absorb fluid from the blood and then begin to degrade. PLA loses roughly 17% of its mass every 16 weeks in vivo [27], and thus will be fully degraded after less than 2 years.

Feasibility Assessment

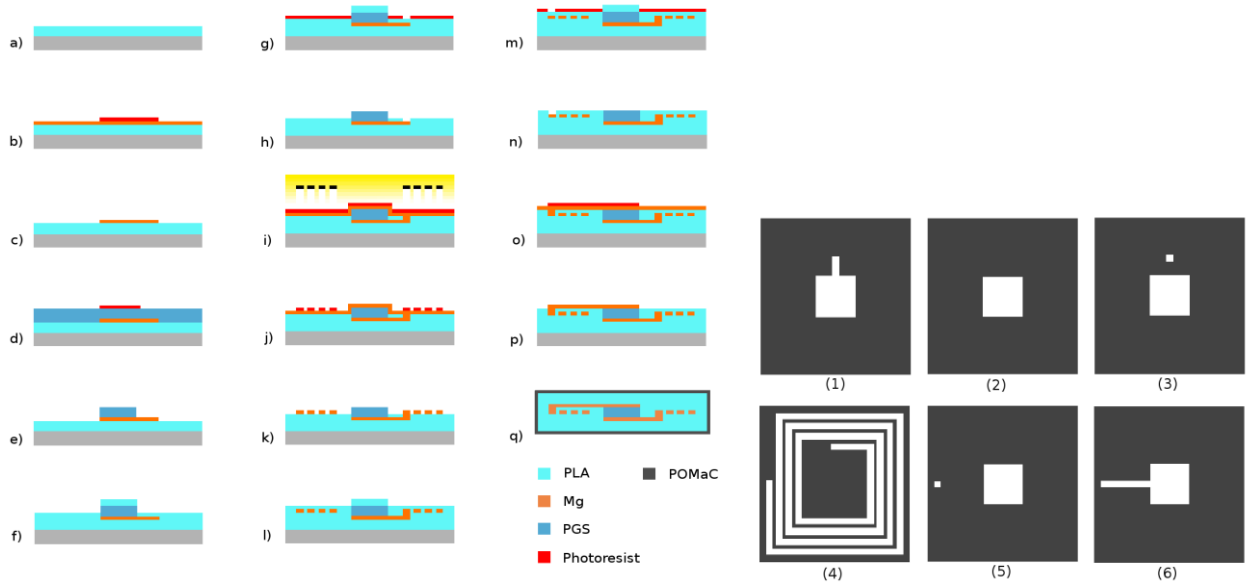

I. Fabrication Process

II. Masks

Figure 10: The proposed fabrication process and masks used :

The proposed fabrication process is shown in figure X, masks used in figure Y:
(a) PLA spin coating on a silicon wafer **(b)** Magnesium vapor deposition (low temperature)[32] and photoresist patterning using mask 1 **(c)** Etching, creating the bottom plate **(d)** Spin coating of PGS, photoresist patterning using mask 2 **(e)** Etching, creating the dielectric **(i)** Spin coating of PLA **(g)** Photoresist patterning using mask 3 **(h)** Etching for contact digging **(i)** Magnesium deposition and photoresist exposure using mask 4 (this step is kept explicit just to illustrate the exposure process, it is implicit in other patterning steps) **(j)** Result after photoresist exposure **(k)** Etching, creating the coil **(l)** Spin coating of PLA **(m)** Photoresist patterning using mask 5 **(n)** Etching for contact digging **(o)** Magnesium deposition and photoresist patterning using mask 6 **(p)** Etching,

Curvature radius

The two limiting aspects when choosing layer thickness for our device were the distance of the Mg plates from the neutral plane and the overall thickness of the PLA layer. PGS and POMaC are elastomers, thus, they didn't add any constraints, compared to the other two materials. Naturally, the capacitor plates couldn't both be located on the neutral plane, additionally the inductance required to be on the neutral plane, so we decided to place the plates symmetrically to the inductance, to minimize the stress for both plates(since the device is symmetric the neutral plane is necessarily at the center).
The critical strain of pure magnesium is around 2-6%[33], assuming a bending radius of 2 mm (imposing a safety margin from the minimum needed bending radius: 3.25 mm from collapsed stent size). Because the capacitor is 6 μm thick (4μm dielectric + 2x1μm plates thickness) the plates would have to withstand the highest stress on the outer side, at 3 μm from the neutral plane, so according to the calculation

$$\varepsilon_{plate} = \frac{h}{R} x100 = \frac{3\mu m}{2mm} x100 = 0.15\%$$

which is well within the comfort zone.
The thickness of the PLA substrate should also be very small, in part due to the mechanical properties of PLA (which can be improved nonetheless, by mixing with other polymers) but mostly not to reduce pressure sensitivity excessively. The theoretical thickness limit due to critical strain (assuming 2% critical strain and 2mm curvature radius as pessimistic hypothesis[34]) is of 40 μm from the neutral plane. While one might be inclined so simply pick a very thin layer for the mentioned reasons doing so would make manipulation and installation of the device harder, thus, as a compromise we picked a half thickness of 30 μm.

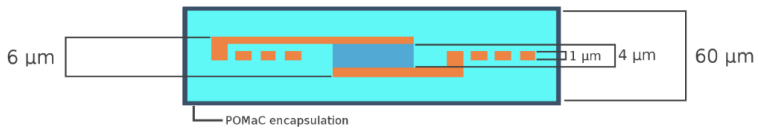

Figure 11 : Layer thickness

This would lead to the deposition of a layer of PLA on top of the plates of thickness 27 μm (30 μm - 3 μm), which would attenuate deformation of the capacitor, however this layer is almost two orders of magnitude thinner than the width of the capacitor (2.5mm/27m ~ 93)which considering the elastic modulus (~1 GPa [34]) suggests the compression of the capacitor should not be too affected, except for near the edges.

Conclusion

The market for this device to detect aortic stenosis in at-risk patients is evident, but such a technology could be applied for other purposes as well. For instance, as biodegradable stents are still a developing technology, this setup could be applied to testing various potential materials. Two pressure sensors--one on the edge of the stent and the other in the middle--would demonstrate whether the tested material effectively widens the pinch point of the artery, due to the difference between the two pressure readings. Another potential application could arise in the future, when biodegradable stents are more commonplace, to conduct post-stenting monitoring and ensure the stent is working properly, rather than relying on the current standard of computed tomography (CT) scans. This device could also find a use in the stenting of aortic coarctation, a congenital defect in children in which the aorta is narrower than normal, and recurrence of coarctation can occur even after stenting; our device would detect if coarctation returns, and thus indicate if further treatment is needed.

Appendix

Teamwork was well divided among our various disciplines for this project. With a background in bioengineering, Brooke lead the search for a biological need which we could fulfill. She continued to aid in this way throughout the project, giving advice on stenting procedures and biocompatibility. Francesco figured out the layout of the device, the process flow and the stress analysis, also creating the relative pictures. Francesco and Brooke worked together on finding appropriate materials for the device which had appropriate material properties, degradation times, and availability for manufacturing techniques.

Stan and Carla were the driving force behind the electronics component of our project, doing many calculations about the necessary frequency and dimensions. This included writing a Matlab program which takes in the many variables of our design and outputs the dielectric thickness, an invaluable tool when designing. Carla performed testing of the Todd-Andrews algorithm with real patient data, and Stan specified how the microcontroller would be integrated. Carla calculated the safe frequency at which our device could communicate via RF, identified the specific absorption rate before concentrating on the external patch and the calculations that it implied. The original figures we use, as well as the design of our device by a 3D printer, were made possible by Carla.

Combining their areas of expertise, Carla and Brooke worked together on analyzing the state of the art devices. All team members helped with then designing an innovative device which differentiates itself from these competitors.

Overall, we all helped each other on most of our various tasks, both giving our expertise when we had it and learning new topics from teammates as well as from the literature.

References:

1. Sharabiani M. T. A., Fiorentino F., Angelini G. D., Patel N. N. Long-term survival after surgical aortic valve replacement among patients over 65 years of age. Open Heart (2016). 3(1).
2. Maganti K., Rigolin V. H., Sarano M. E., Bonow R. O. Valvular heart disease: diagnosis and management. Mayo Clin Proc (2010). 85(5): 483-500.
3. Rao P. S. Long-term follow-up results after balloon dilation of pulmonic stenosis, aortic stenosis, and coarctation of the aorta: a review. Prog. Cardiovasc. Disc. (1999). 42(1): 59-74.
4. Caldara M., Nodari B., Re V., Bonandrini B. Miniaturized blood pressure telemetry system with RFID interface. Procedia Engineering (2014). 344-347.
5. Chen X., Assadsangabi B., Hsiang Y., Takahata K. Enabling angioplasty-ready "smart" stents to detect in-stent restenosis and occlusion. Adv. Sci. (2018). 5(5): 1700560.
6. Gore Medical. Gore announces successful patient implant of endovascular stent graft for the ascending aorta [press release]. (27 August 2018). Retrieved from www.goremedical.com.
7. Li R., Wang L., Yin L. Materials and devices for biodegradable and soft biomedical electronics. Materials (2018). 11(11): 2108.
8. Boutry C. M., Nguyen A., Lawal Q. O., Chortos A., Rondeau-Gagne S., Bao Z. A sensitive and biodegradable pressure sensor array for cardiovascular monitoring. Adv Mater Res (2015). 27(43): 6954-6961.
9. Dr. Rodney Stramel, personal interview. 14 December 2018.
10. Cremer J., Teebken O. E., Simon A., Hutzelmann A., Heller M., Haverich A. Thoracic computed tomography prior to redo coronary surgery. Eur. J. Cardiothorac. Surg. (1998). 13(6): 650-654.
11. P. Vaillancourt, A. Djemouai, J.F. Harvey, M. Sawan, "*EM radiation behavior upon biological tissues in a radio-frequency power transfer link for a cortical visual implant*", in : Proc. IEEE EMBS Conf., vol. 6, 1997, pp 2499-2500.
12. E. Freudenthal, D. Herrera, F. Hautz, C. Natividad, A. Ogrey, J. Sipla, A. Sosa, C. Betancourt, L. Estevez, "*Evaluation of HF RFID for implanted medical applications*", Departmental Technical Reports (CS),2007, Paper 162
13. Aubert, H. "*RFID technology for human implant devices*". C. R. Phys. 2011, 12, 675–683.
14. Nataraj V., Mortimer A. J. Endovascular abdominal aortic aneurysm repair. Continuing Educ. Anaesth. Crit. Care Pain (2004). 4(3): 91-94.
15. Dielectric parameters for various tissues of the human body : https://www.fcc.gov/general/body-tissue-dielectric-parameters
16. ICNIRP Guidelines, "*For limiting exposure to time-varying electric, magnetic and electromagnetic fields (up to 300 GHz)*", published in : Health Physics 74 (4), 494-522, 1998.
17. Erbel R., Eggebrecht H. Aortic dimensions and the risk of dissection. Heart (2006). 92(1): 137-142.
18. Huang Y., Wong Y. S., Ng H. C. A., Boey F. Y. C., Venkatraman S. Translation in cardiovascular stents and occluders: from biostable to fully degradable. Bioeng Transl Med (2017). 2(2): 156-169.
19. Hwang, S. W., Park, G., Cheng, H., Song, J. K., Kang, S. K., Yin, L., Rogers, J. A. (2014). 25th anniversary article: Materials for high-performance biodegradable semiconductor devices. *Advanced Materials*, *26*(13), 1992-2000.
20. Heer L. M., Budde R. P. J., Mali W. P. T. M., Vos A. M., Herwerden L. A., Kluin J. Aortic root dimension changes during systole and diastole: evaluation with ECG-gated multidetector row computed tomography. Int. J. Cardiovasc. Imaging. (2011). 27(8): 1195-1204.
21. Bhagat V., Becker M. L. Degradable adhesives for surgery and tissue engineering. Biomacromolecules (2017). 18(10): 3009-3039.

22. Matsuda T., Nakajima N., Itoh T., Takakura T. Development of a compliant surgical adhesive derived from novel fluorinated hexamethylene diisocyanate. ASAIO Trans. (1989). 35(3): 381-383.
23. Kocka V., Widimsky P. The bioresorbable stent in perspective - how much of an advance is it? Interv. Cardiol. Rev. (2014). 9(1): 23-25.
24. Huang X. Bioresorbable materials and their application in electronics. Elements in Flexible and Large-Area Electronics (2017). Cambridge: Cambridge University Press.
25. Bell T. Electrical conductivity of metals (2018). Retrieved from www.thebalance.com
26. Shasteen C., Choy Y. B. Controlling degradation rate of poly(lactic acid) for its biomedical applications. Biomed. Eng. Lett. (2011). 1: 163-167.
27. Zhang Z., Cui H. Biodegradability and biocompatibility study of poly(chitosan-g-lactic acid) scaffolds. Molecules (2012). 17(3): 3243-3258.
28. [xxx] MSP432P4111IPZ Datasheet "MSP432P411x, MSP432P401x SimpleLinkTMMixed-Signal Microcontrollers" , Texas instruments ,decembre 2007
29. [xxx] M.Willemet, P. Chowienczyk, J. Alastruey, "A database of virtual healthy subjects to assess the accuracy of foot-to-foot pulse wave velocities for estimation of aortic stiffness" , Department of Clinical Pharmacology ,juin 2015
30. Zhang B., Montgomery M., Chamberlain D., Ogawa S., Korolj A., Pahnke A., Wells L., Massé S., Kim J., Reis L., Momen A., Nunes S., Wheele A., Nanthakumar K., Keller G., Sefton M., Radisic M. Biodegradable scaffold with built-in vasculature for organ-on-a-chip engineering and direct surgical anastomosis - Supplementary Information. Nature Materials 15, 669-678 (2016)
31. Tran R., Thevenot P., Gyawali D., Chiao J., Tang L., Yang J., Synthesis and characterization of a biodegradable elastomer featuring a dual crosslinking mechanism, Soft Matter 11 (2010)
32. Bountry C., Kaizawa Y., Schroeder B., Chortos A., Legrand A., Wang Z., Chang J., Fox P., Bao Z., A stretchable and biodegradable strain and pressure sensor for orthopaedic application, Nature Electronics 1, 314-321(2018)
33. Properties of magnesium and alloys http://www.totalmateria.com/Article138.htm
34. Farah S., Anderson D., Langer R., Physical and mechanical properties of PLA, and their functions in widespread applications - A comprehensive review. Advanced Drug Delivery Reviews 107, 367-392 (2016)